Available online at www.sciencedirect.com
ScienceDirect
Quaternary Research 67 (2007) 128–135
QUATERNARY RESEARCH
www.elsevier.com/locate/yqres

Inception of the Northern European ice sheet due to contrasting ocean and insolation forcing

Bjørg Risebrobakken [a,b,*], Trond Dokken [a], Odd Helge Otterå [a,c], Eystein Jansen [a,b], Yongqi Gao [a,c], Helge Drange [a,c]

[a] Bjerknes Centre for Climate Research, Allégaten 55, 5007 Bergen, Norway
[b] Department of Earth Science, University of Bergen, Allégaten 41, 5007 Bergen, Norway
[c] Nansen Environmental and Remote Sensing Centre, Thormøhlensgt. 47, 5006 Bergen, Norway

Received 9 August 2005
Available online 10 October 2006

Abstract

About 115,000 yr ago the last interglacial reached its terminus and nucleation of new ice-sheet growth was initiated. Evidence from the northernmost Nordic Seas indicate that the inception of the last glacial was related to an intensification of the Atlantic Meridional Overturning Circulation (AMOC) in its northern limb. The enhanced AMOC, combined with minimum Northern hemisphere insolation, introduced a strong sea–land thermal gradient that, together with a strong wintertime latitudinal insolation gradient, increased the storminess and moisture transport to the high Northern European latitudes at a time when the Northern hemisphere summer insolation approached its minimum.

Keywords: Glacial inception; Nordic Seas; Northern European ice sheets; Paleo-reconstruction: OGCM; AMOC; Insolation; Insolation gradient

Introduction

Due to the general acceptance of the orbital (or Milankovitch) theory, there is a basic understanding of the fundamental drivers of the glacial cycles. The specific feedbacks that are involved in the triggering or inception process of a glacial cycle remain, however, to a large degree elusive. A common conceptual view is that the inception was initiated by lowered summer insolation at high northern latitudes, which cooled the Nordic Seas and other high latitude oceans, and which in turn provided snow and sea-ice feedbacks that accelerated cooling by a freshening of the surface ocean and concomitant reduction of the Atlantic Meridional Overturning Circulation (AMOC) (Cortijo et al., 1994; Imbrie et al., 1992). Contradicting this scenario, we here show by a combination of paleo-reconstructions and General Circulation Model (GCM) results from the Bergen Climate Model (BCM) that the strength of the AMOC apparently increased in its northern limb at the end of the last interglacial (marine isotope sub-stage (MIS) 5.5: ~126,000–115,000 yr), at the time when major ice sheets nucleated. Our results indicate that nucleation of the Northern European ice sheets was a result of the specific orbital forcing at that time, coexisting with an enhanced AMOC, increased winter precipitation, lowered snow melting due to reduced summer insolation, and related feedbacks.

Materials and methods

Paleo-reconstructions

Three sediment cores have been studied at high temporal resolution through the MIS 5.5 and the MIS 5.5/5.4 transition. All cores were obtained at IMAGES cruises with R/V Marion Dufresne. MD95-2010 is from the Vøring Plateau, whereas MD99-2303 and MD99-2304 are from the Fram Strait (Fig. 1). They are located to reflect changes in extent and variability of Atlantic Water transport towards the Arctic. Risebrobakken et al. (2005) determined the marine isotope stage 5 age models of the cores through stable isotope correlation towards the chronology established on the NEAP18K core (Chapman and Shackleton, 1999). The same age

* Corresponding author. Bjerknes Centre for Climate Research, Allégaten 55, N-5007 Bergen, Norway. Fax: +47 55584330.
E-mail address: bjorg.risebrobakken@bjerknes.uib.no (B. Risebrobakken).

0033-5894/$ - see front matter © 2006 University of Washington. All rights reserved.
doi:10.1016/j.yqres.2006.07.007

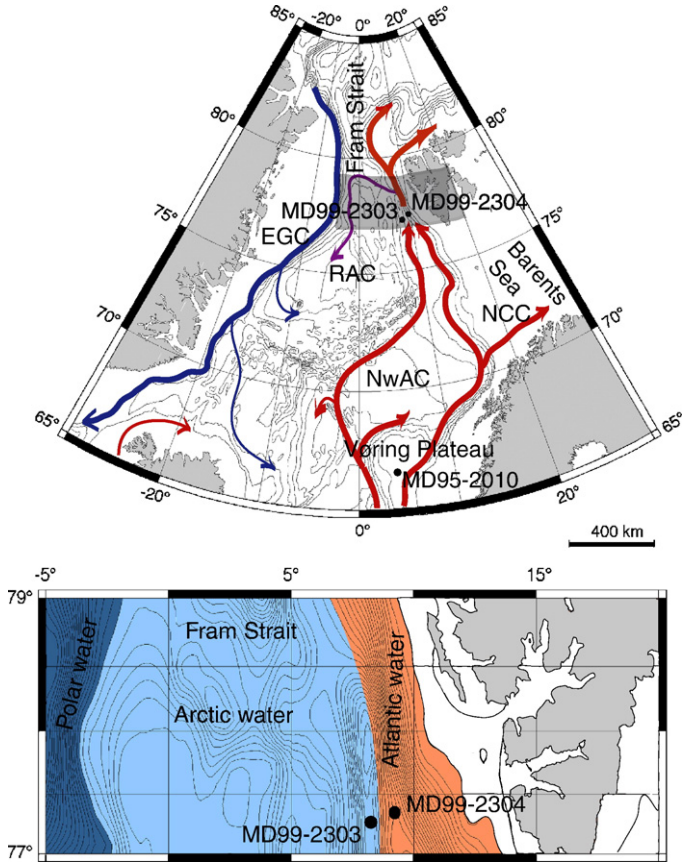

Figure 1. The main surface currents in the Nordic Seas and locations of the studied cores (MD95-2010 (66°41.05′N, 04°33.97′E: 1226 m water depth), MD99-2304 (77°37.26′N, 09°56.90′E: 1315 m water depth) and MD99-2303 (MD99-2303; 77°31.18′N, 08°23.98′E: 2277 m water depth)) are shown in the upper panel. NwAC = Norwegian Atlantic Current, NCC = North Cape Current, RAC = Return Atlantic Current and EGC = East Greenland Current. The bathymetry is indicated by isolines every 500 m. The distribution of the surface water masses in the Fram Strait is indicated in the lower panel, representing the area indicated by the grey square in the upper panel.

models have been used in this study, and detailed information on the procedure can be found in Risebrobakken et al. (2005). The studied time interval, 126,000 – 110,000 yr, is represented by 32 cm in MD95-2010 (1227.5 – 1259.5 cm core depth), 171 cm in MD99-2304 (2086.5 – 2257.5 cm core depth) and 31 cm in MD99-2303 (904.5 – 935.5 cm core depth). All three cores were sampled every cm throughout the studied time interval, giving approximate time resolutions of 500 yr (MD95-2010 and MD99-2303) and 100 yr (MD99-2304).

Stable isotope measurements were performed every cm on the left coiling form of *Neogloboquadrina pachyderma* (150–500 μm fraction), using Finnigan MAT 251 and MAT 252 mass spectrometers at the GMS lab at the University of Bergen, both equipped with automatic preparation lines ("Kiel device"). The samples were crushed and cleaned with methanol in an ultrasonic bath before being measured. All results are reported in ‰ vs. VPDB.

The present number of minerogenic grains >0.5 mm has been counted every cm in all cores through the studied time interval. These grains are assumed to be ice rafted, and they are presented as number of grains/gram sediment.

The number of planktonic foraminifers was counted at irregular intervals at the 150–500 μm fraction (26, 56 and 20 samples in MD99-2303, MD99-2304 and MD95-2010, respectively). A minimum of 300 foraminifers was counted from each sample, if possible (in MD99-2303, MD99-2304 and MD95-2010 this is valid for 14, 44 and 8 samples, respectively). The assemblages were separated into *N. pachyderma* sinistral and dextral, *Globigerina quinqueloba* and other planktonic species. The relative abundance of *N. pachyderma* (s), *N. pachyderma* (d) and *G. quinqueloba* were calculated for all samples with a total of more than 100 planktonic foraminifers (in MD99-2303, MD99-2304 and MD95-2010 this is valid for 20, 51 and 20 of the counted samples, respectively).

Model experiments

The applied model system consists of a global version of MICOM (Bleck et al., 1992), fully coupled to a dynamic (Harder, 1996) and thermodynamic (Drange and Simonsen, 1996) sea ice module. The model is configured with a local horizontal orthogonal grid system with one pole over North America and the other pole over central Europe (Bentsen et al., 1999). The horizontal grid resolution in the North Atlantic/Nordic Seas region is about 40 km in experiment E1, and 80 km in experiments E2 and E3. For all model experiments there are 26 vertical layers, of which the uppermost mixed layer (ML) has a temporally and spatially varying density. The

specified potential densities of the subsurface layers are chosen to ensure a proper representation of the major water masses in the North Atlantic/Nordic Seas region. Furthermore, the bathymetry is computed as the arithmetic mean value based on the ETOPO-5 database (NOAA, 1988). The experiments are initialized with climatological temperature (Levitus and Boyer, 1994) and salinity (Levitus et al., 1994) fields, a two-meter-thick sea ice cover based on the climatological sea ice extent, and an ocean at rest. For experiment E1, the model set-up and integration follows the synoptic hindcast simulations in Furevik et al. (2002). The model was then integrated for 30 yr by applying the monthly mean NCEP/NCAR atmospheric forcing fields, and thereafter forced by the daily NCEP/NCAR reanalysis fields (Kalnay et al., 1996) for the period 1948–1996. From the NCEP/NCAR reanalysis the wind stress, short wave, long wave, latent and sensible heatfluxes, precipitation, runoff and sea level pressure (SLP) fields were used. During the spinup phase, the ML temperature and salinity were relaxed towards the monthly mean climatological values of Levitus and Boyer (1994) and Levitus et al. (1994), with a relaxation time scale of 30 days for a 50-m-thick ML. The relaxation was reduced linearly with ML thicknesses exceeding 50 m, and it was set to zero in waters where sea ice was present in March (September) in Arctic (Antarctic) to avoid relaxation towards temperature and salinity outliers in the poorly sampled polar waters. For the integration with daily fields, freshwater fluxes, diagnosed from the salinity relaxation with climatological fields, were added to the ML.

For experiment E2 and E3, the model setup and integration is described in Otterå and Drange (2004). The initialization is the same as above, and the spinup period for this model setup was 420 yr where relaxation was applied on both temperature and salinity. For years 400–420, the mean weekly freshwater relaxation fluxes were diagnosed and stored. The model was then run for a further 80-yr period with temperature relaxation switched off, whereas the salinity relaxation was reduced by increasing the relaxation time scale from 30 days to 2 yr. In addition to this, the diagnosed freshwater fluxes were added to the ML. From year 500 we then start three sensitivity experiments, one with orbital configuration as 125,000 yr BP (E2), one as 115,000 yr BP (E3) and one for present day (control case, no changes made). The use of weak relaxation of salinity and the diagnosed freshwater fluxes ensures that the strength of the AMOC remains fairly stable in the control case, and that that temperature and salinity anomalies are free to develop, propagate and decay in the sensitivity experiment. Furthermore, for all simulations, the momentum, heat and freshwater fluxes are modified when the modeled surface state differs from the NCEP/NCAR reanalysis surface state by a bulk parameterization scheme (Bentsen, 2002). Using this configuration, it has been shown that the model system captures the main features of the observed water mass exchanges between the North Atlantic and the Nordic Seas in a realistic manner (Nilsen et al., 2003).

To simulate the extreme high and low values in high latitude summer insolation in E2 and E3, the orbital parameters (eccentricity, obliquity and perihelion) are set at the values for 125,000 yr and 115,000 yr, respectively. The NCAR/NCEP downward solar irradiance is then modified by a latitude-time-dependant factor f according to $f=S_x/S_p$, where S_p and S_x are the solar insolation calculated for the present-day situation (Kutzbach and Gallimore, 1988), and for the sensitivity experiments E2 and E3, respectively. Using this factor gives about a 6% (10–12%) decrease (increase) in summer solar irradiance at 60°N at 115,000 yr (125,000 yr) compared to the present day (Otterå and Drange, 2004).

Results and discussion

The large-scale $\delta^{18}O$ pattern is determined by global sea-level changes, whereas the superimposed variability of each record is the result of local temperature and salinity conditions. The last interglacial is clearly present at all three sites (Fig. 2a). Relative abundance of the foraminifer species provides information on temperature changes. Decreases in % *N. pachyderma* (sin), the only polar species, indicate increased influence of warmer water masses, also indicated by increased percentages of the subpolar species (*N. pachyderma* (dex) and *G. quinqueloba*). Thus, MD95-2010 (Vøring Plateau) and MD99-2304 (eastern Fram Strait) show generally warm interglacial conditions throughout MIS 5.5 (Figs. 2b–d), with relative abundances comparable to Holocene values at the Vøring Plateau (Andersson et al., 2003) and in the eastern Fram Strait (Hald et al., 2004). The foraminifer data show that the early phase of the interglacial was warm at both MD95-2010 and MD99-2304 followed by somewhat colder conditions. This pattern can possibly be linked to the general reduction of the Northern Hemisphere (NH) summer insolation. In the late MIS 5.5, decreasing percentages of *N. pachyderma* (sin) indicate, however, renewed sea-surface temperature (SST) warming when the NH summer insolation approached its minimum. Contemporaneously with this SST increase, the amounts of the planktic foraminifer *G. quinqueloba* increased in MD99-2304 (Fig. 2d). As this species is associated with the Arctic front (Johannessen et al., 1994), this implies that the Arctic front migrated eastwards towards MD99-2304. MD99-2303, located west of MD99-2304, contains a high-productive, dominantly polar foraminifer fauna throughout MIS 5.5 (Fig. 2), indicating a location underneath Arctic water (Johannessen et al., 1994). MD99-2304 shows lower planktonic $\delta^{13}C$ values than MD99-2303 throughout MIS 5.5 (Fig. 2e), supporting the interpretation of a different water mass and lower productivity at that site. It has been shown that Atlantic water is characterized by lower $\delta^{13}C$ values than Arctic water (Johannessen et al., 1994).

The signature of the two nearby cores are different; however, we find no reason not to trust any of the results. The $\delta^{18}O$ records are comparable for all three sites and there is a strong similarity between the IRD records. The $\delta^{13}C$ records indicate different water masses, and the core with highest sedimentation rate shows both highest diversity of foraminifer species and lowest total foraminifer content. Neither of these would have been the case if one of the sites were influenced by bioturbation, any other sediment disturbances or dissolution.

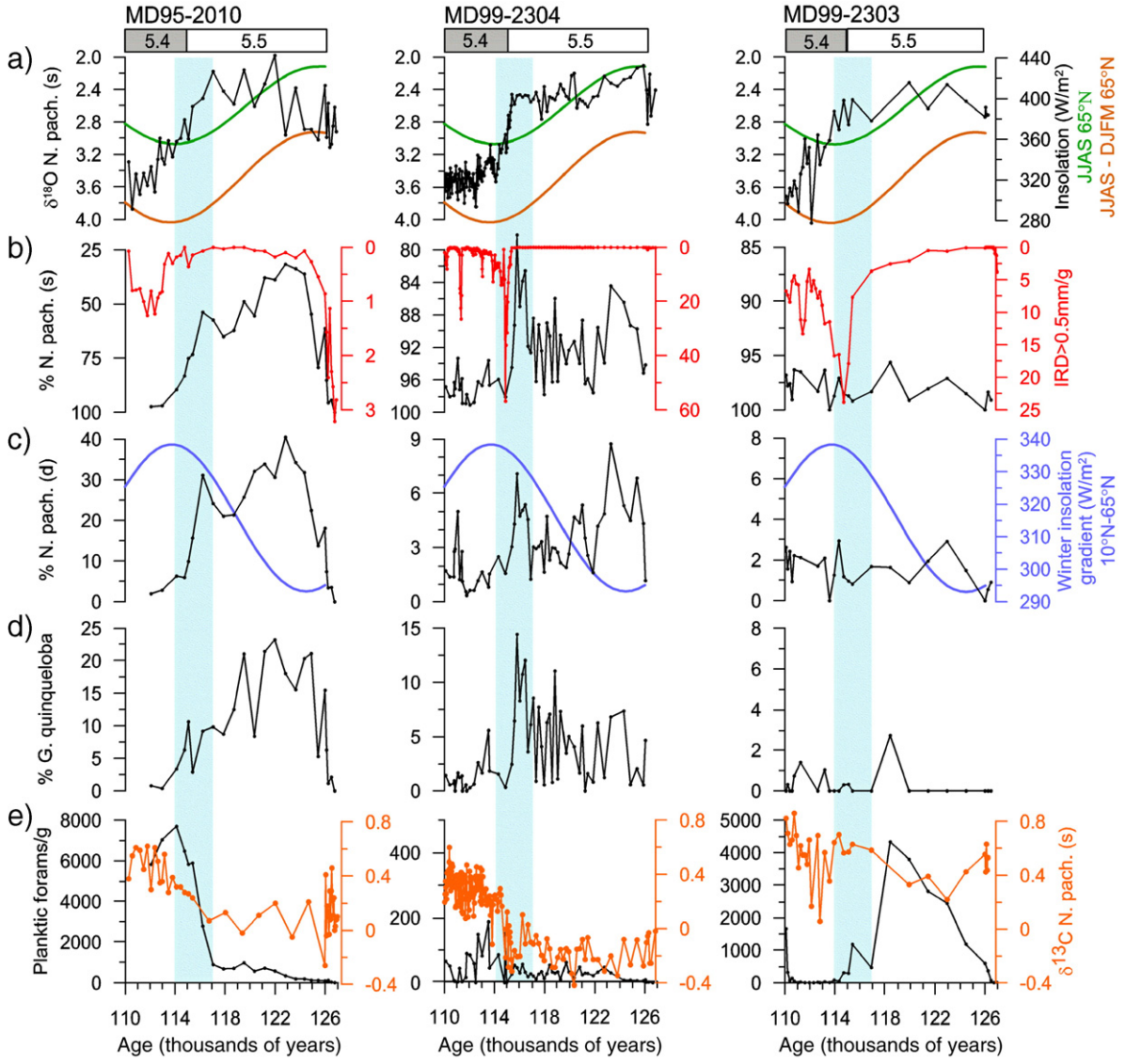

Figure 2. Downcore records from the studied cores and insolation parameters data (Laskar, 1990). Note scale differences between similar records from different cores, resulting from the different oceanographic regimes represented by the cores and vicinity to available IRD sources. Horizontal bars indicate the isotope stages. Vertical bars highlight the transitional phase between the interglacial and the glacial onset, as given by this study (117,000–114,000 yr). (a) *N. pachyderma* (s) $\delta^{18}O$ records from the cores (black), mean summer (June–September) insolation at 65°N (green) and the difference between mean summer (June–September) and mean winter (December to March) insolation at 65°N (brown). (b) % *N. pachyderma* (s) (NPS) in the cores (black) (all foraminifer counts were performed at the 150–500 μm fraction) and number of Ice Rafted Debris (IRD) >500 μm/g sediment (red). (c) % *N. pachyderma* (d) (NPD) in the cores (black) and the mean winter (December-March) insolation gradient between 10°N and 65°N (blue). (d) % *G. quinqueloba* in the cores. (e) Total number of planktic foraminifers/g sediment in the cores (black) and *N. pachyderma* (s) $\delta^{13}C$ records from the cores (orange).

We believe that the Arctic front was located between the sites, dividing the Arctic water from a laterally restricted wedge of Atlantic water that was present in the easternmost part of the Fram Strait. This argument is supported by the present day surface interface between Atlantic and Arctic water masses, located between/near these sites and determined by the strong bathymetric gradient (Fig. 1) (Manley, 1995; Quadfasel et al., 1987). Atlantic water influence both sites; however, the high temperature and salinity core of the West Spitsbergen Current is located between the 200-m and 1500-m depth contours, thus influencing MD99-2304 whereas MD99-2303 is located west of this zone (Quadfasel et al., 1987). From 116,000 yr, both cores show the same Arctic water characteristics. The significantly increased foraminifer abundance recorded by MD95-2010 indicates that Arctic water also covered this site at that time (Fig. 2e).

Thus, at the end of the last interglacial there was a simultaneous warming of and lateral restriction of the Norwegian Atlantic Current/West Spitsbergen Current. A similar response of this current regime, with an intensification of the slope current and an eastward confinement of the Atlantic water, has been observed as a function of strong westerlies during the recent decades (Blindheim et al., 2000; Dickson et al., 2000). The late MIS 5.5 warming might therefore be the result of prevailing, strong westerlies providing enhanced warm water transport towards the Arctic.

Another plausible response to increased westerlies is an enhanced Ekman transport of warm water into the Barents Sea. This type of response is demonstrated in the simulated northward volume transport through the Barents Sea Opening (BSO) in the ocean model experiment (E1), where the model is forced with observed (NCEP reanalysis) atmospheric forcing for the period 1948–1996. Associated with a stronger net inflow through the BSO, the Icelandic low extends more northeast into the central Nordic Seas (increasing the westerlies), where the changes in the SLP, associated with one standard deviation change in the BSO volume transport index, exceeds 3 hPa (where 1 hPa=0.1 kPa) (Fig. 3a). Near the Azores, one standard deviation change in the BSO volume transport index correspond to a 3-hPa change in the SLP. An increased net transport of Atlantic water through the Fram Strait and the BSO, forced by a prevailing low pressure anomaly and strong westerlies in the Nordic Seas, has also been documented by studies of instrumental records (Dickson et al., 2000; Loeng et al., 1997). It is therefore likely that the enhanced Atlantic water influx at the end of MIS 5.5 introduced rather warm SSTs and open-water masses in the Barents Sea as well as in the Fram Strait. The occurrence of a warm marine mollusc fauna in Arctic Russian sediments of MIS 5.5 age also indicates strong inflow of Atlantic water to the Barents Sea (Funder et al., 2002; Mangerud et al., 1998, 1999; Raukas, 1991).

Northern Hemisphere summer insolation is considered to be a major forcing factor behind glacial-interglacial cycles (Imbrie et al., 1992, 1993). Through MIS 5.5 the summer insolation decreased from an extreme high to reach a profound minimum at 115,000 yr. To assess likely impacts of the orbital forcing on the ocean circulation, we investigated the response of the AMOC to reduced insolation in order to resemble the situation at 125,000 yr and 115,000 yr with the ocean–sea ice model. The obtained results show that the modeled AMOC intensified in response to the lower summer insolation at high northern latitudes (Fig. 3b). Less sea ice melted during the summer season, providing saltier waters to the high northern latitudes and an intensified overturning circulation (Otterå and Drange, 2004). Warm conditions also existed in the North Atlantic at the end of MIS 5.5 (Cortijo et al., 1994; Duplessy and Shackleton, 1985; McManus et al., 2002; Ruddiman and McIntyre, 1979). In previous studies, however, the Nordic Seas have been considered as cold at this time (Cortijo et al., 1994). Both our paleo-reconstructions and model results, on the contrary, strongly indicate that the effect of an enhanced AMOC was noticeable in the northernmost Nordic Seas and the Barents Sea. The increased presence of the warm Atlantic water is probably a combined result of enhanced westerly wind forcing and increased salinity due to less summer sea-ice melting as the insolation forcing decreased. The late MIS 5.5 warming was probably not picked up in previous studies due to low temporal resolution and the locations of the studied cores, which were positioned too far to the west to capture the relatively narrow wedge of northward flowing warmer water. Sirocko et al.

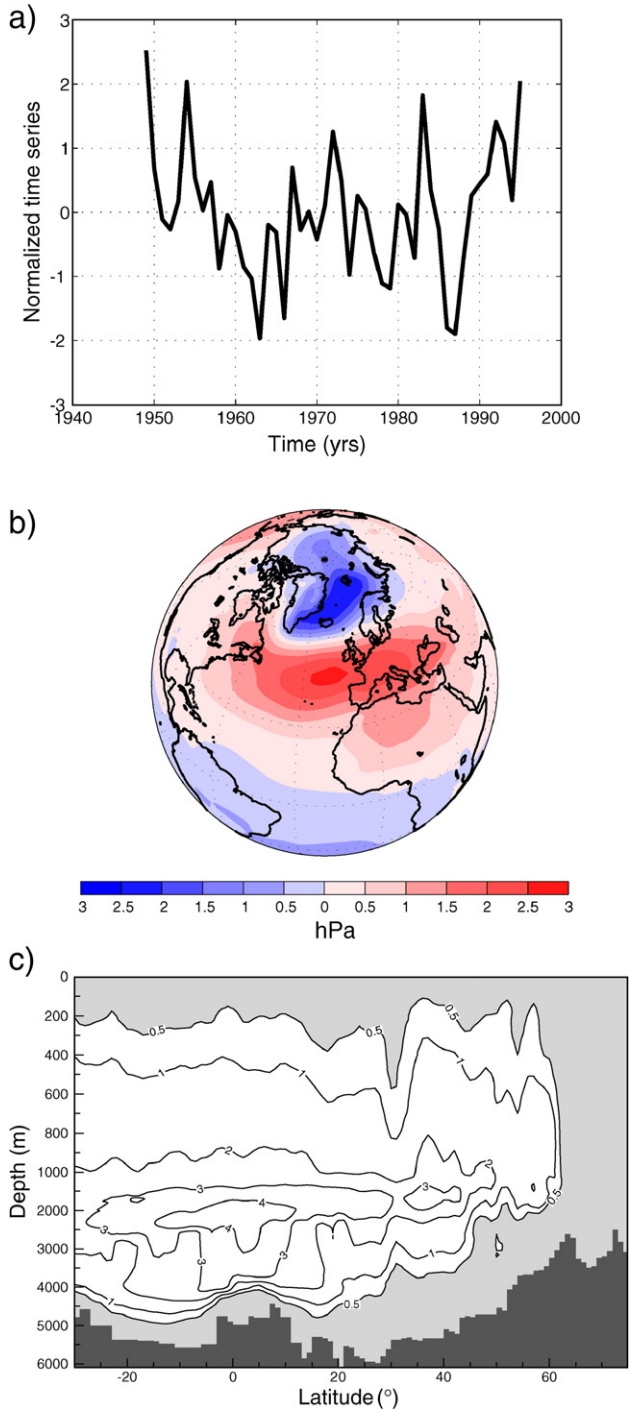

Figure 3. Modeled oceanic responses to atmospheric forcing and NH insolation. (a) Normalized and detrended time series of the simulated winter (DJFM) mean volume transport through the BSO for the period 1948–1996. (b) Regression of the observed winter (DJFM) mean NCEP/NCAR SLP field on the normalized simulated winter (DJFM) volume transport through the BSO for the period 1948–1996 for zero lag. The SLP field is detrended before applying the regression. The regression values (in hPa) correspond to the typical anomaly associated to one standard deviation of the BSO volume transport index. (c) Changes in the simulated zonally averaged annual mean steamfunction values (Sv) for the Atlantic basin for the last glacial inception shown as the difference between E3 and E2 (E3–E2, see methods), where the NCAR/NCEP downward solar irradiances in E2 and E3 are modified to reflect the insolation values at 125,000 yr and 115,000 yr, respectively (Otterå and Drange, 2004).

(2005), however, has detected an aridity pulse in central Europe at the time of the last glacial inception. A strong northern low SLP field at winter will probably correspond with an equally strong high SLP winter field reaching towards central Europe, introducing dry and cold conditions in that region. Thus, decreased precipitation in central Europe is a plausible response to the atmospheric regime that we postulate, and the central European aridity pulse may be seen as supportive evidence for our hypothesis.

The latitudinal moisture flux from low to high latitudes is a function of the latitudinal insolation gradient, with an increased moisture flux when the insolation gradient increases (Raymo and Nisancioglu, 2003). The low-to-high latitude wintertime insolation gradient increased through the glacial inception phase (Fig. 2c). Thus, the moisture transport towards the high north increased both due to the strong ocean–land thermal gradient, the result of enhanced AMOC/warm SSTs and decreasing high latitude insolation, and the increasing latitudinal insolation gradient. The moist maritime air masses combined with the cold atmospheric temperatures led to excess winter snow and reduced summer melting. This was probably essential for the onset of glacial growth, by introducing a strong positive glacial mass balance. An albedo feedback from the increased snow cover probably further amplified the cooling effect, and under the prevailing conditions the glaciers grew and ice sheets could nucleate.

The noticeable increase in % *N. pachyderma* (sin), indicating cooling, after the late MIS 5.5 warm phase coincides with the first major IRD input at 116,000 yr (Fig. 2b). According to the present chronology, this first IRD peak coincides with the first onset of global sea-level fall and ice-volume change after the interglacial (Chapman and Shackleton, 1999; Stirling et al., 1998). Sea-level changes are expressed in $\delta^{18}O$ records, and the response to increased global ice volume is also seen in the corresponding increase in $\delta^{18}O$ (Fig. 2a). The IRD found in MD99-2303 and MD99-2304 most probably originated from Spitsbergen (Risebrobakken et al., 2005), and more IRD is seen closer to this source. Consequently, glaciers at Spitsbergen were large enough to reach the coastline and initiate significant calving before major global ice-sheet growth is observed. Terrestrial evidence also support an early inception of glaciation at Spitsbergen (Mangerud et al., 1998). This area was therefore implicated in the earliest inception phase of the major ice sheets of the last glacial. The minor IRD content found in MD95-2010 probably originated from areas where a limited Scandinavian Ice Sheet (SIS) reached the coast.

During the last glacial period, the growth and decay of the SIS and the Barents-Kara Sea Ice Sheet (BKIS) were not synchronous. The BKIS had an early maximum extent, corresponding with a much more limited SIS ice extent (Baumann et al., 1995; Svendsen et al., 2004). This asymmetric behavior with an early inception and large expansion in the region south of the Barents-Kara Seas is supported by our results. The probable presence of warm late MIS 5.5 SSTs in the Barents Seas introduced a similar strong land-sea thermal gradient in Arctic Russia as in the Spitsbergen region. The wind forcing and wintertime latitudinal insolation gradient would also provide excess winter precipitation over northern Russia, which was met with reduced summer melting due to the insolation minimum. As the summer insolation forcing decreased, the tree line was forced southward in an east–west asymmetric pattern, with a larger shift in Siberia than in Scandinavia (Crucifix and Loutre, 2002). This diminished the forest snow masking effect (Bonan et al., 1992) and increased the surface albedo throughout the year, which further amplified the cooling effect. Eventually ice sheets nucleated, and a self-intensifying albedo feedback was maintained. We postulate that a stable glacial regime was established on land during the inception phase. Prevailing favorable conditions for maintaining this glacial state caused the ice sheet to expand and ground at the epicontinental Barents and Kara Seas as global sea level fell. The BKIS reached its maximum position at approximately 90,000 yr (Svendsen et al., 2004). A falling sea level and ice-sheet expansion over the Barents Sea eventually introduced an obstacle for the transport of Atlantic water into the Barents Sea, and so moisture transport to northern Russia was prevented. This development may have been important for the ice-sheet distribution later in the last glaciation, restricting the BKIS when the SIS reached its maximum position.

If the Nordic Seas were covered by an increasingly more stable and perennially lasting sea-ice cover during the inception phase, as previously believed, both Spitsbergen and northern Russia would be concealed from the moisture influx essential for major glacial growth. Existence of a warm sea surface in the Fram Strait and the Barents Sea during the inception phase provides us with a scenario that may explain the existence of large ice sheets in this area in the first phase of the glacial period. Thus, we conclude that the glacial inception was not due to a reduction of the AMOC, but rather the opposite, a result of the confluence of increased influence of the AMOC in the Arctic/sub-Arctic and its associated maritime climate, together with reduced summer insolation and an enhanced moisture flux driven by an increased wintertime latitudinal insolation gradient.

The climate history of the present interglacial is in many ways comparable with MIS 5.5, and the present conditions in Northern Europe do in some ways fulfill requirements for glacial inception. Even at its present minimum position the Northern Hemisphere summer insolation is, however, fundamentally different from the situation 115,000 yr ago. The insolation fall during the Holocene has been less than half of the fall during MIS 5.5. The present value is also 40 W/m^2 higher than the values at 115,000 yr. Together with the high levels of greenhouse gases, this difference in insolation forcing is probably the main factor preventing glacial inception today.

Acknowledgments

Rune Søraas, Odd Hansen, Dag Inge Blindheim, Helge Hellevang and Werner Svellingen are thanked for laboratory assistance and help with sample preparation. We thank Kerim Nisancioglu, Jan Mangerud and Jerry McManus for providing comments to an early version of the manuscript, and Øyving Lie for discussions during the review process. Svante Björck

and three other anonymous referees are thanked for their review of the manuscript. This is publication Nr A141 from the Bjerknes Centre for Climate Research.

References

Andersson, C., Risebrobakken, B., Jansen, E., Dahl, S.O., 2003. Late Holocene surface–ocean conditions of the Norwegian Sea (Vøring Plateau). Paleoceanography 18, 1044, doi:10.1029/2001PA000654.

Baumann, K.-H., Lackschewitz, K.S., Mangerud, J., Spielhagen, R., Wolf-Welling, T.C.W., Henrich, R., Kassens, H., 1995. Reflection of Scandinavian Ice Sheet Fluctuations in Norwegian Sea Sediment during the past 150,000 years. Quaternary Research 43, 185–197.

Bentsen, M., 2002. Modelling Ocean Climate Variability of the North Atlantic and the Nordic Seas. PhD thesis, Department of Mathematics and Nansen Environmental and Remote Sensing Centre, Bergen, Norway.

Bentsen, M., Evensen, G., Drange, H., Jenkins, A.D., 1999. Coordinate transformation on a sphere using conformal mapping. Monthly Weather Review 127, 2733–2740.

Bleck, R., Rooth, C., Hu, D., Smith, L.T., 1992. Salinity-driven thermohaline transients in a wind- and thermohaline-forced isopycnic coordinate model of the North Atlantic. Journal of Physical Oceanography 22, 1486–1515.

Blindheim, J., Borovkov, V., Hansen, B., Malmberg, S.A., Turrell, W.R., Østerhus, S., 2000. Upper layer cooling and freshening in the Norwegian Sea in relation to atmospheric forcing. Deep-Sea Research I 47, 655–680.

Bonan, G.B., Pollard, D., Thompson, S.L., 1992. Effects of boreal forest vegetation on global climate. Nature 359, 716–718.

Chapman, M.R., Shackleton, N.J., 1999. Global ice-volume fluctuations, North Atlantic ice-rafting events, and deep-ocean circulation changes between 130 and 70 ka. Geology 27, 795–798.

Cortijo, E., Duplessy, J.C., Labeyrie, L., Leclaire, H., Duprat, J., van Weering, T.C.E., 1994. Eemian cooling in the Norwegian Sea and North Atlantic ocean preceding continental ice-sheet growth. Nature 372, 446–449.

Crucifix, M., Loutre, M.F., 2002. Transient simulations over the last interglacial period (126–115 kyr BP): feedback and forcing analysis. Climate Dynamics 19, 417–433.

Dickson, R.R., Osborne, T.J., Hurrell, J.W., Meincke, J., Blindheim, J., Adlandsvik, B., Vinje, T., Alekseev, G., Maslowski, W., 2000. The Arctic Ocean response to the North Atlantic oscillation. Journal of Climate 13, 2671–2696.

Drange, H., Simonsen, K., 1996. Formulation of air–sea fluxes in the ESOP2 version of MICOM. Technical Report Nansen Environmental and Remote Sensing 125.

Duplessy, J.C., Shackleton, N.J., 1985. Response of global deep-water circulation to Earth's climatic change 135,000–107,000 years ago. Nature 316, 500–507.

Funder, S., Demidov, I., Yelovicheva, Y., 2002. Hydrography and mollusc of the Baltic and the White Sea-North Sea seaway in the Eemian. Palaeogeography, Palaeoclimatology, Palaeoecology 184, 275–304.

Furevik, T., Bentsen, M., Drange, H., Johannessen, J.A., Korablev, A., 2002. Temporal and spatial variability of the sea surface salinity in the Nordic Seas. Journal of Geophysical 107, doi:10.1029/2001JC001118.

Hald, M., Ebbesen, H., Forwick, M., Godtliebsen, F., Khomenko, L., Korsun, S., Ringstad Olsen, L., Vorren, T.O., 2004. Holocene paleoceanography and glacial history of the West Spitsbergen area, Euro-Arctic margin. Quaternary Science Reviews 23, 2075–2088.

Harder, M., 1996. Dynamik, Rauhigkeit und Alter des Meereises in der Arktis. PhD thesis, Alfred Wegner Institut für Polar- und Meeresforsch., Bremerhaven, Germany.

Imbrie, J., Boyle, E.A., Clemens, S.C., Duffy, A., Howard, W.R., Kukla, G., Kutzbach, J., Martinson, D.G., McIntyre, A., Mix, A.C., Molfino, B., Morley, J.J., Peterson, L.C., Pisias, N.G., Prell, W.L., Raymo, M.E., Shackleton, N.J., Toggweiler, J.R., 1992. On the structure and origin of major glaciation cycles 1. Linear responses to Milankovitch forcing. Paleoceanography 7, 701–738.

Imbrie, J., Berger, A., Boyle, E.A., Clemens, S.C., Duffy, A., Howard, W.R., Kukla, G., Kutzbach, J., Martinson, D.G., McIntyre, A., Mix, A.C., Molfino, B., Morley, J.J., Peterson, L.C., Pisias, N.G., Prell, W.L., Raymo, M.E., Shackleton, N.J., Toggweiler, J.R., 1993. On the structure and origin of major glaciation cycles 2. The 100,000-year cycle. Paleoceanography 8, 699–735.

Johannessen, T., Jansen, E., Flatøy, A., Ravelo, A.C., 1994. The relationship between surface water masses, oceanographic fronts and paleoclimatic proxies in surface sediments of the Greenland, Iceland, Norwegian Seas. In: Zahn, R., Kominski, M., Labyrie, L. (Eds.), Carbon Cycling in Glacial Ocean: Constraints on the Ocean's Role in Global Change. Springer-Verlag, New York, pp. 61–85. NATO ASI Series.

Kalnay, E., Kanamitsu, M., Kistler, R., Collins, W., Deaven, D., Gandin, L., Iredell, M., Saha, S., White, G., Woollen, J., Zhu, Y., Chelliah, M., Ebisuzaki, W., Higgins, W., Janowiak, J., Mo, K.C., Ropelewski, C., Wang, J., Leetmaa, A., Reynolds, R., Jenne, R., Joseph, D., 1996. The NCEP/NCAR 40-year reanalysis project. Bulletin of the American Meteorological Society 77, 437–471.

Kutzbach, J.E., Gallimore, R.G., 1988. Sensitivity of a coupled atmosphere/mixed layer ocean model to changes in orbital forcing at 9000 years B.P. Journal of Geophysical Research 93, 803–821.

Laskar, J., 1990. The chaotic motion of the solar system: a numerical estimate of the chaotic zones. Icarus 88, 266–291.

Levitus, S., Boyer, T.P., 1994. World Ocean Atlas 1994, NOAA Atlas NESDIS 4. Temperature, vol. 4. US Gov. Printing Office, Washington D.C., USA.

Levitus, S., Burgett, R., Boyer, T.P., 1994. World Ocean Atlas 1994, NOAA Atlas NESDIS 3. Salinity, vol. 3. US Gov. Printing Office, Washington D.C., USA.

Loeng, H., Ozhigin, V., Ådlandsvik, B., 1997. Water fluxes through the Barents Sea. ICES Journal of Marine research 54, 310–317.

Mangerud, J., Dokken, T., Hebbeln, D., Heggen, B., Ingólfsson, Ó., Landvik, J.Y., Mejdahl, V., Svendsen, J.I., Vorren, T.O., 1998. Fluctuations of the Svalbard–Barents sea ice sheet during the last 150 000 years. Quaternary Science Reviews 17, 11–42.

Mangerud, J., Svendsen, J.I., Astakhov, V.I., 1999. Age and extent of the Barents and Kara ice sheets in Northern Russia. Boreas 28, 46–80.

Manley, T.O., 1995. Branching of Atlantic Water within the Greenland-Spitsbergen passage: An estimate of recirculation. Journal of Geophysical Research 100, 20627–20634.

McManus, J.F., Oppo, D.W., Keigwin, L.D., Cullen, J.L., Bond, G.C., 2002. Thermohaline circulation and prolonged interglacial warmth in the North Atlantic. Quaternary Research 58, 17–21.

Nilsen, J.E.Ø., Gao, Y., Drange, H., Furevik, T., Bentsen, M., 2003. Simulated North Atlantic-Nordic Seas water mass exchanges in an isopycnic coordinate OGCM. Geophysical Research Letters 30, 1531, doi:10.1029/2002GL016597.

NOAA. (1988). Data Announcement 88-Mgg-02, Digital relief of the surface of the Earth. Tech. Rep., NOAA, National Geophysical Data Centre, Boulder, Colorado, USA.

Otterå, O.H., Drange, H., 2004. Effects of solar irradiance forcing on the ocean circulation in the North Atlantic in an isopycnic coordinate OGCM. Tellus Series A-Dynamic Meteorology and Oceanography 56, 154–166.

Quadfasel, D., Gascard, J.-C., Koltermann, K.-P., 1987. Large-scale oceanography in fram strait during the 1984 marginal ice zone experiment. Journal of Geophysical Research 92, 6728–9719.

Raukas, A., 1991. Eemian interglacial record in the Northwestern European part of the Soviet Union. Quaternary International 10–12, 183–189.

Raymo, M.E., Nisancioglu, K., 2003. The 41 kyr world: Milankovitch's other unsolved mystery. Paleoceanography 18, 1011.

Risebrobakken, B., Dokken, T., Jansen, E., 2005. The extent and variability of the meridional Atlantic circulation in the Nordic Seas during marine isotope stage 5 and its influence on the inception of the last glacial. In: Drange, H., Dokken, T., Furevik, T., Gerdes, R., Berger, W.H. (Eds.), The Nordic Seas: An Integrated Perspective. AGU Geophysical Monograph, vol. 158, pp. 323–339.

Ruddiman, W.F., McIntyre, A., 1979. Warmth of the subpolar North Atlantic Ocean during Northern hemisphere ice-sheet growth. Science 204, 173–175.

Sirocko, F., Seelos, K., Schaber, K., Rein, B., Dreher, F., Diehl, M., Lehne, R., Jëger, K., Krbetschek, M., Degering, D., 2005. A late Eemian aridity

pulse in central Europe during the last glacial inception. Nature 436, 833–836.

Stirling, C.H., Esat, T.M., Lambeck, K., McCulloch, M.T., 1998. Timing and duration of the last interglacial: Evidence for a restricted interval of widespread coral reef growth. Earth and Planetary Science Letters 160, 745–762.

Svendsen, J.I., Alexanderson, H., Astakhov, V.I., Demidov, I., Dowdeswell, J.A., Funder, S., Gataullin, G., Henriksen, M., Hjort, C., Houmark-Nielsen, M., Hubberten, H.W., Ingólfsson, Ó., Jakobsson, M., Kjær, K.H., Larsen, E., Lokrantz, H., Lunkka, J.P., Lyså, A., Mangerud, J., Matiouchkov, A., Murray, A., Möller, P., Nisessen, F., Nikolskaya, O., Polyak, L., Saarnisto, M., Siegert, C., Siegert, M.J., Spielhagen, R.F., Stein, R., 2004. Late Quaternary ice sheet history of Northern Eurasia. Quaternary Science Reviews 23, 1229–1271.